UC Berkeley
UC Berkeley Previously Published Works

Title
Sex- and mutation-specific p53 gain-of-function activity in gliomagenesis.

Permalink
https://escholarship.org/uc/item/9w45x5fn

Journal
Cancer Research Communications, 1(3)

Authors
Rockwell, Nathan
Yang, Wei
Warrington, Nicole
et al.

Publication Date
2021-12-01

DOI
10.1158/2767-9764.crc-21-0026

Peer reviewed

eScholarship.org Powered by the California Digital Library
University of California

CANCER RESEARCH COMMUNICATIONS

AACR American Association for Cancer Research

RESEARCH ARTICLE https://doi.org/10.1158/2767-9764.CRC-21-0026 OPEN ACCESS

Sex- and Mutation-Specific p53 Gain-of-Function Activity in Gliomagenesis

Nathan C. Rockwell[1], Wei Yang[2], Nicole M. Warrington[1], Max V. Staller[2,3], Malachi Griffith[2,4,5,6], Obi L. Griffith[2,4,5,6], Christina A. Gurnett[7], Barak A. Cohen[2,8], Dustin Baldridge[1], and Joshua B. Rubin[1,9]

ABSTRACT

In cancer, missense mutations in the DNA-binding domain of *TP53* are common. They abrogate canonical p53 activity and frequently confer gain-of-oncogenic function (GOF) through localization of transcriptionally active mutant p53 to noncanonical genes. We found that several recurring p53 mutations exhibit a sex difference in frequency in patients with glioblastoma (GBM). *In vitro* and *in vivo* analysis of three mutations, $p53^{R172H}$, $p53^{Y202C}$, and $p53^{Y217C}$, revealed unique interactions between cellular sex and p53 GOF mutations that determined each mutation's ability to transform male versus female primary mouse astrocytes. These phenotypic differences were correlated with sex- and p53 mutation–specific patterns of genomic localization to the transcriptional start sites of upregulated genes belonging to core cancer pathways. The promoter regions of these genes exhibited a sex difference in enrichment for different transcription factor DNA-binding motifs. Together, our data establish a novel mechanism for sex-specific mutant p53 GOF activity in GBM with implications for all cancer.

Significance: Sex differences in cancer, including glioblastoma, have been observed in both incidence and outcome. We reveal that *TP53*, the most commonly mutated gene in cancer, contributes to sex differences through differential GOF activity. This discovery has critical implications for our understanding of p53 mutations and the importance of sex as a biological variable.

Introduction

The tumor suppressor *TP53* (p53), which regulates cell-cycle progression, DNA damage repair, apoptosis, and stem cell differentiation (1), is the most commonly mutated gene in cancer (2). It functions through direct protein–protein interactions and acting as a positive or negative regulator of transcription through its canonical DNA-binding site (3, 4). p53's transcriptional activity is dependent on many interacting and context-specific factors such as the tissue or cell type, the mechanism of p53 activation, and the severity and longevity of DNA damage (5). A growing body of evidence indicates that sex has a profound influence on the role of p53 in development, disease, and aging. In mice and rats, loss of p53 *in utero* results in decreased female progeny compared with males – as a consequence of aberrant X-inactivation in females and altered X-gene dosage – which result in embryonically lethal neural tube defects (6, 7).

p53 also exhibits sex differences in the maintenance of neural progenitor cells (NPC) in the subventricular zone (8). Under normal conditions, post pubertal male mice NPCs are depleted faster than in female mice. Knocking out p53 in NPCs protects against depletion in males suggesting a male-specific proapoptotic function of p53 in NPCs (8).

Regardless of the geographic region, human females consistently exhibit greater longevity than males and other mammals (9). Work in *Drosophila* has shown that germline overexpression of wild-type (WT) p53 decreased lifespan in females and increased lifespan in males. Tissue-specific overexpression of WT p53 in the central nervous system had the opposite effect, increasing lifespan in females while decreasing lifespan in males (10). Together, these findings demonstrate that p53 activity is both sex and tissue dependent.

Sex differences in the effects of p53 mutations have also been observed in cancer. Overall, in nonreproductive tumors, p53 mutations occur more frequently in males, and are associated with worse survival (11). However, in individuals with Li-Fraumeni syndrome (LFS), a familial cancer predisposition syndrome associated with germline pathogenic variants in p53, females have an overall increased risk of developing cancer compared with males (12). For some other

[1]Department of Pediatrics, Washington University School of Medicine, St. Louis, Missouri. [2]Department of Genetics, Washington University School of Medicine, St. Louis, Missouri. [3]Center for Computational Biology, University of California, Berkeley, Berkeley, California. [4]McDonnell Genome Institute, Washington University School of Medicine, St. Louis, Missouri. [5]Division of Oncology, Department of Medicine, Washington University School of Medicine, St. Louis, Missouri. [6]Siteman Cancer Center, Washington University School of Medicine, St. Louis, Missouri. [7]Department of Neurology, Washington University School of Medicine, St. Louis, Missouri. [8]The Edison Family Center for Genome Sciences and Systems Biology, Washington University in St. Louis School of Medicine, St. Louis, Missouri. [9]Department of Neuroscience, Washington University School of Medicine, St Louis, Missouri.

Corresponding Author: Joshua B. Rubin, Washington University in St. Louis, Campus Box 8208, 660 South Euclid Avenue, St. Louis, MO 63110. Phone: 314-286-2790; E-mail: rubin_j@wustl.edu

doi: 10.1158/2767-9764.CRC-21-0026

This open access article is distributed under the Creative Commons Attribution 4.0 International (CC BY 4.0) license.

© 2021 The Authors; Published by the American Association for Cancer Research

cancers, such as brain tumors, males with LFS exhibit higher risk. Mice harboring a germline mutant p53 and loss of the promyelocytic leukemia gene, exhibit sex differences in cancer type and survival. Male mice develop more soft tissue sarcomas and have shortened survival compared with females, who are more likely to develop osteosarcomas and exhibit longer survival (13). In a model of glioma, we previously observed that codeletion of p53 and the tumor suppressor neurofibromin 1 (*Nf1*) is sufficient for transformation of male, but not female astrocytes (14). Knocking out *Nf1* and p53 in NPCs *in utero* also leads to faster glioma formation and disease progression in male mice than female mice (15).

The most common p53 alterations in cancer are missense mutations in the DNA-binding domain (DBD; ref. 16). In addition to the loss of canonical DNA binding and gene regulation, many p53 missense mutations exhibit gain-of-function (GOF) and are more oncogenic than *TP53* deletion (17). Many of these neomorphic functions can be attributed to p53–DNA interactions at noncanonical binding sites that drive the aberrant expression of oncogenes and repression of tumor suppressors (18). The specific activity of different p53 mutations has been shown to be mediated by novel interactions with other proteins (such as NF-κB, ETS2, and NF-Y) and differential genomic localization (19). Despite efforts to specify GOF-mutant p53 phenotypes, characterizing the effects of mutant p53 GOF on transcription and tumorigenicity has been complicated by disparities in reported results, suggesting that, much like WTp53, mutant p53 activity, even for the same missense mutation, is diverse and context dependent.

Given the known sex differences in p53 function and cancer incidence and survival, it is important to consider whether p53 GOF mutations contribute to sex differences in cancer (20). Many of the pathways that contribute to sex differences including metabolism, cell-cycle progression, invasion and epithelial-to-mesenchymal transition, epigenetic dysregulation, and immunity (20), are associated with mutant p53 GOF activity. However, the influence of sex on mutant p53 GOF activity remains unknown. In glioblastoma (GBM), males have been shown to have both increased incidence and decreased overall survival compared with females (21). Notably, *TP53* is among the most mutated genes in GBM with most mutations occurring as missense mutations in the DBD (22). Therefore, the intersection of sex differences in p53 function, sex difference in GBM incidence and outcome, and the high rate of p53 missense mutations in GBM make this an ideal system for interrogating the effects of sex on p53 GOF activity with potential applicability to p53 GOF mutations in all cancer.

Materials and Methods

Animal Studies Approval

Study was approved in accordance with an animal studies protocol (no. 2018205) approved by the Animal Studies Committee of Washington University School of Medicine per the recommendations of the NIH Guide for the Care and Use of Laboratory Animals.

Analysis of Missense Mutations Across Cancer

TP53 mutation data was aggregated from multiple studies (Supplementary Table S1). The frequency of missense mutations in the DBD was calculated as a fraction of the total p53 mutations in the dataset. Significance was calculated using Fisher exact test between each cancer type and the pan-cancer data set.

Meta-analysis of Mutation Incidence in Glioblastoma

TP53 mutation data was collected for 552 male and 442 female patients from The Cancer Genome Atlas (TCGA 2013), the Catalog of Somatic Mutations in Cancer (COSMIC– ALL CNS), and International Agency for Research on Cancer (IARC) datasets. The absolute number of mutations at each codon in the *TP53* gene was quantified for each sex independently, and the sex ratio determine by dividing the number of male tumors with a mutation by female tumors with a mutation for each codon. Significant sex differences in mutation frequency were determined for each codon using Fisher exact test ($P < 0.05$).

Primary Mouse Astrocyte Isolation and Culture

Trp53$^{f/-}$ pups were produced by mating male *Trp53*$^{-/-}$ mice (B6.129S2-Trp53tm1Tyj/J – The Jackson Laboratory #002101) with *Trp53*$^{f/f}$ mice (B6.129P2-Trp53tm1Brn/J – The Jackson Laboratory #008462). Primary astrocytes were isolated from postnatal day 1 pups as previously described (14). The sex of the pups was determined by PCR of genomic DNA for *Jarid1c*/*Jarid1d*[14].

Forward: 5′-CTGAAGCTTTTGGCTTTGAG-3′
Reverse: 5′-CCACTGCCAAATTCTTTGG-3′

Astrocytes from at least three male and three female pups were combined for each male and female.

Immunocytochemistry/Immunofluorescence

Astrocytes were plated on poly-L-lysine (ScienCell) coated coverslips and fixed with 3.2% paraformaldehyde for 10 minutes at room temperature. Fixed cells were immunolabeled for GFAP and p53 (Methods, Table 1). Nuclei were counterstained with DAPI and mounted on microscope slides using Immu-Mount (Thermo Fisher Scientific). Images were taken using a fluorescent microscope (Olympus Bx60) and processed using Zeis Zen 3.1 software.

DNA Plasmids, Cloning, and Virus Production

Mouse *Trp53* transcript variant 1 (NM_011640.3) was cloned into the retroviral vector pMSCV-IRES-GFP II (Addgene plasmid #52107). *Trp53* point mutations were introduced using site-directed mutagenesis with the Q5 Site-Directed Mutagenesis Kit (New England Biolabs E0552S). Retrovirus was produced by plasmid transfection into Platinum-E (Plat-E) cells. Lentivirus to express Cre recombinase was produced by transfecting NIH HEK293T cells with Cre-IRES-PuroR plasmid (Addgene plasmid #30205), Δ8.9 and VSV-G. All transfections were performed with FuGENE 6 transfection agent (Promega E2691) in Opti-MEM Reduced Serum Medium (Gibco 31985070) for 5 hours, and the media replaced with standard DMEM/F12, 10% FBS for viral production. Virus was collected 48, 72, and 96 hours posttransfection and combined.

Primary Astrocyte Genomic Alteration

Trp53$^{mutantp53/-}$ astrocytes were produced by transduction with mutant p53-IRES-eGFP retrovirus followed by subsequent transduction with Cre-IRES-Puro lentivirus. Briefly, postnatal day 1 *Trp53*$^{f/-}$ astrocytes were transduced with a 1:1 ratio of viral media and growth media for 48 hours. Following stable expression of eGFP, cells were sorted by flow-sort for eGFP-positive cells. Sorted astrocytes were transduced with a 1:1 ratio of lentiviral-Cre-IRES-puro virus and growth media for 48 hours. Astrocytes were then selected for 1 week in 2.5 μg/mL puromycin (Sigma P8833). *Trp53*^{KO} astrocytes was achieved by transduction with lentiviral-Cre-IRES-puro virus and selection for 1 week

TABLE 1 Antibodies used in this study.

Antibody	Antigen	Host	Source	Application	Dilution
2524	Mouse p53	Mouse	Cell Signaling Technology	Western blot	1:1,000
				ChIP	5 μg antibody/25 μg DNA
				ICC	1:2,000
SC-365062	GAPDH	Mouse	Santa Cruz	Western blot	1:200
P53-CM5P-L	P53	Rabbit	Leica	IHC	1:200
13-0300	GFAP	Rat	Invitrogen	ICC	1:250
E0431	Rabbit Immunoglobulin	Swine	Dako	IHC – Secondary/Biotin	1:750
926-32212	Mouse IgG	Donkey	LI-COR	Western blot – Secondary/IRDye 800CW	1:50,000
A11077	Rat IgG	Goat	Invitrogen	ICC – Secondary/Fluor 568	1:1,000

in 2.5 μg/mL puromycin. All primary astrocytes were transfected three passages postisolation. Cells were tested for *Mycoplasma* contamination by PCR (ATCC #30-1012K). All assays were performed between 4 and 15 passages after puromycin selection.

Western Blot Analysis

Total cell lysates were collected in RIPA buffer supplemented with proteinase and phosphatase inhibitors (Roche 11697498001, Roche 04906937001). Protein was separated by electrophoresis using 4%–12% gradient Bis-Tris NuPAGE gels (Invitrogen) and transferred to a nitrocellulose membrane. Membranes were blocked using Odyssey blocking buffer diluted 1:1 in 0.1% PBST. Membranes were then incubated in primary antibodies diluted in blocking buffer overnight at 4°C, followed by secondary antibodies diluted in blocking buffer for 1 hour at room temperature. Blots were imaged using the Bio-Rad ChemiDoc MP Imager and analyzed using the Bio-Rad Image Lab Software V6.1. Primary and secondary antibodies and their corresponding dilution factors can be found in Methods in Table 1.

In Vitro Growth Assay

3,000 cells were plated in triplicate in 10 mL media in 10-cm tissue culture plates. After incubation in normal tissue culture conditions for 8 days, the cells were washed with 1× PBS and fixed with 100% methanol at room temperature for 6 minutes. Plates were air dried at room temperature. Cells were stained for 1 hour at room temperature with Giemsa stain (Sigma GS500) diluted 1:20 in dH_2O. Stained plates were washed three times in dH_2O for 5 minutes at room temperature and air dried before imaging using the Imagescanner III (GE Healthcare). Growth was determined by percentage area of the plate covered by cells using ImageJ v1.52a. The global scale was set according to the width of a plate (10 cm), the image flattened, and the color channels split. Using the green channel only, the background was subtracted from each image, and the threshold set to 235 for each image. A circle of equal size was selected with each plate and the total percent area calculated using the "analyze particles" tool. Within each experiment, the percent area for each plate was normalized to the average of the Male KO plates. To test for interactions between sex and genotypes on the normalized growth rates, mixed effect linear regression models were used using the lmerTest R package, with variances controlled for the technical replicates within each plate. Regression terms included sex, the tested genotype, and their interaction.

In Vivo Tumorigenesis: Flank Implantations

Flank tumors were generated by implanting mutant p53 astrocytes subcutaneously into the left- and right-side flanks of NCr nude mice (Taconic). Male and female astrocytes were trypsinized and resuspended in DMEM/F12, and combined at a 1:1 ratio with Matrigel. One-hundred microliters of cell/Matrigel suspension equaling 750,000 male or female cells were injected into opposite flanks of 3 male and 3 female hosts. Flank tumors size was measured weekly using a digital caliper until the largest tumors reached a terminal volume of 1 cm^3.

RNA Sequencing

Total RNA was isolated using the RNeasy Mini Kit (Qiagen) from *Trp53* KO or *Trp53*-mutant astrocytes. Samples were prepared according to library kit manufacturer's protocol, indexed, pooled, and sequenced on an Illumina HiSeq. Basecalls and demultiplexing were performed with Illumina's bcl2fastq software and a custom python demultiplexing program with a maximum of one mismatch allowed in the indexing read. RNA-sequencing (RNA-seq) reads were then aligned to the Ensembl release 76 primary assembly with STAR version 2.5.1a (23). Gene counts were derived from the number of uniquely aligned unambiguous reads by Subread:featureCount version 1.4.6-p5 (24). Isoform expression of known Ensembl transcripts were estimated with Salmon version 0.8.2 (25). Sequencing performance was assessed for the total number of aligned reads, total number of uniquely aligned reads, and features detected. The ribosomal fraction, known junction saturation, and read distribution over known gene models were quantified with RseQC version 2.6.2 (26).

All gene counts were then imported into the R/Bioconductor package EdgeR (27) and TMM normalization size factors were calculated to adjust for samples for differences in library size. Ribosomal genes and genes not expressed in the smallest group size minus one sample greater than one count-per-million were excluded from further analysis. The TMM size factors and the matrix of counts were then imported into the R/Bioconductor package Limma (28). Weighted likelihoods based on the observed mean-variance relationship of every gene and sample were then calculated for all samples with the voomWithQualityWeights (29). The performance of all genes was assessed with plots of the residual SD of every gene to their average log-count with a robustly fitted trend line of the residuals. Differential expression analysis was then performed to analyze for differences between conditions and the results were filtered for only those genes with Benjamini–Hochberg false-discovery rate adjusted *P* values less than or equal to 0.05. Interactions between sex and gene expressions were tested using the limma package.

Sparse Principal Component Analysis

Sparse principal component analysis (PCA) was performed on normalized gene counts using R/SparsePCA v0.1.2 (30) and variance plotted using the R package

plot3D v1.3. Normalized gene counts for all genes with nonzero sparse loadings for the each of the first three principal components were used to generate heat maps. Heat maps were generated using R/heatmap3 v1.1.9.

Pathway Analysis

GOF transcriptomes were defined as all genes that were differentially expressed between p53-mutant and p53 KO astrocytes (FDR < 0.05) within each sex. The GOF gene lists were then compared between males and females within each mutation to define the sex-specific and shared GOF transcriptomes. Pathway enrichment analysis was performed on shared and sex-specific differentially expressed gene lists using ShinyGO v0.65 (31). Enrichment analysis is based on hypergeometric distribution followed by FDR correction.

Whole-Exome Sequencing

Whole genomic DNA was isolated from 10^6 cells using the QIAamp DNA Mini Kit (Qiagen 51304). gDNA was fragmented, indexed, and pool. Indexed pools were hybridized with Agilent SureSelectXT Mouse All Exon kit per manufacturer's instructions and sequenced on an Illumina NovaSeq-6000. Reads were analyzed using a DRAGEN Bio-IT processor (version 0 × 18101306) running software version 07.021.602.3.8.4. FASTQ files were mapped to mouse reference mm10 and output in CRAM format with duplicates marked. Hard filtered variants in the mouse exome target region were annotated with snpEff v4.3t.

Chromatin Immunoprecipitation Sequencing

10 million astrocytes were fixed with 1% formaldehyde in DMEM/F12 for 10 minutes are room temperature with gentle rocking. Fixation was quenched by adding glycine to a final concentration of 125 mmol/L. Cells were washed with cold PBS, scraped into 5 mL cold PBS supplemented with protease inhibitors (PI), phosphatase inhibitors (PPI), and phenylmethylsulfonylfluoride (PMSF), and transferred to 15 mL conical tubes. Cell suspension were pelleted by centrifugation at 4°C for 5 minutes at 1,000 × *g* and resuspended in 1 mL Farnham lysis buffer (plus PI, PPI, and PMSF) for 10 minutes with gentle vortexing every two minutes to isolate nuclei. Nuclei were pelleted by centrifugation at 4°C, for 5 minutes at 2,000 rpm. The nuclear pellet was resuspended in 1 mL RIPA buffer (plus PI, PPI, and PMSF). Sonication was performed on an Epishear probe-in sonicator (Active Motif) at 50% amplitude for 15 cycles of 10 seconds, with 20 seconds of rest between each cycle. Immunoprecipitation was performed as previously described, with an antibody recognizing mouse p53 (see Methods, Table 1).

Sequencing reads were generated using Illumina NovaSeq S4 (2 × 150bp) and processed using the ENCODE Transcription Factor and Histone ChIP-Seq processing pipeline v1.1.6 (http://github.com/ENCODE-DCC/chip-seq-pipeline2). The pipeline filtered and mapped reads to the Mus musculus genome (mm10), validated the quality of the data, and generated fold change signal tracks over the inputs using MACS2. Signal tracks of fold enrichment were visualized with the WashU Epigenome browser (https://epigenomegateway.wustl.edu). Motif search for peaks near gene transcript starting sites was conducted using Hypergeometric Optimization of Motif EnRichment (HOMER, v4.8.3; http://homer.ucsd+.edu/homer/index.html).

IHC of Mouse Tumors

Mouse flank tumors were dissected, drop fixed in 4% paraformaldehyde overnight at 4°C, and transferred to 30% sucrose. Tumors were imbedded in a paraffin block, sectioned, and mounted on microscope slides. Histologic features were determined by hematoxylin and eosin staining. IHC was performed against mouse p53. Antibodies and dilutions are listed in Methods in Table 1. IHC signal was developed with the ImmPACT DAB Peroxidase Kit (Vector Laboratories, SK-4105).

Statistical Analysis

All *in vitro* experiments were carried out at least three times using cells from three independent thaws and platings. Comparisons between mutation frequencies were determined by Fisher exact test. Two-tailed Student *t* test was used for direct comparisons between mutants in the growth assay and tumor volumes. Differences in tumor growth rate were determined by two-way ANOVA. A *Pe* < 0.05 was considered statistically significant. Correlations between mutational burden and proliferation were calculated using Pearson correlation. Statistics were calculated using GraphPad Prism version 9.0.1.

Antibodies

Antibodies used in this study are listed in Table 1

Unique Materials Availability

Male and female astrocyte cultures null for p53 or expressing p53-mutant constructs are primary cultures of limited passage number. These will be freely shared upon request pending availability.

Data Accessibility Statement

All sequencing data are available through GEO via accession number GSE188710: https://www.ncbi.nlm.nih.gov/geo/query/acc.cgi?acc=GSE188710

Results

Sex Differences in the Incidence of p53 Mutations in GBM

Across cancer, *TP53* mutations are most commonly missense mutations in the DBD compared with deletions, inactivating (truncating mutations), or missense mutations outside of the DBD. In patients with LFS, central nervous system (CNS) tumors in particular are significantly associated with germline mutations in the helix-loop-helix region of the DBD, suggesting that these mutations preferentially predispose LFS patients to brain tumors (32). To further investigate the association between mutant p53 in CNS tumors and glioblastoma (GBM), we asked whether this pattern was also present for somatic p53 mutations. *TP53* mutation data were aggregated from multiple studies deposited in the cBioPortal database, including the pan-cancer MSK-IMPACT Clinical Sequencing Cohort and all available studies for glioblastoma, pan-CNS cancers, and the top five cancer types by incidence: breast, lung, skin, pancreatic, and colorectal (33). A complete list of studies and cancer subtypes included in this analysis can be found in Supplementary Table S1. We analyzed the frequency of missense mutations in the DBD as a percentage of all p53 mutations (Fig. 1A and B). Despite the DBD contributing 48% of the amino acids in the full-length p53 protein, missense mutations in the DBD account for 61.5% of p53 mutations in the pan-cancer dataset. In comparison with pan-cancer, missense mutations in the DBD are significantly more frequent in GBM (72.1%, $P = 0.0001$, Fisher exact test), CNS tumors (76.8%, $P < 0.0001$), and colon cancer (66.4%, $P = < 0.0001$), significantly less frequent in breast cancer (56.5%, $P < 0.0001$), and skin cancer (52.5%, $P = 0.0015$), and equally common in prostate (61.4%) and lung cancers (61.7%). In total, missense mutations in the DBD were observed in 19.7% of GBM cases, compared with inactivating mutations in 7.6% and complete deletion in 1%. Together, these data support an enhanced impact of missense mutations in the p53 DBD on GBM and CNS tumor development.

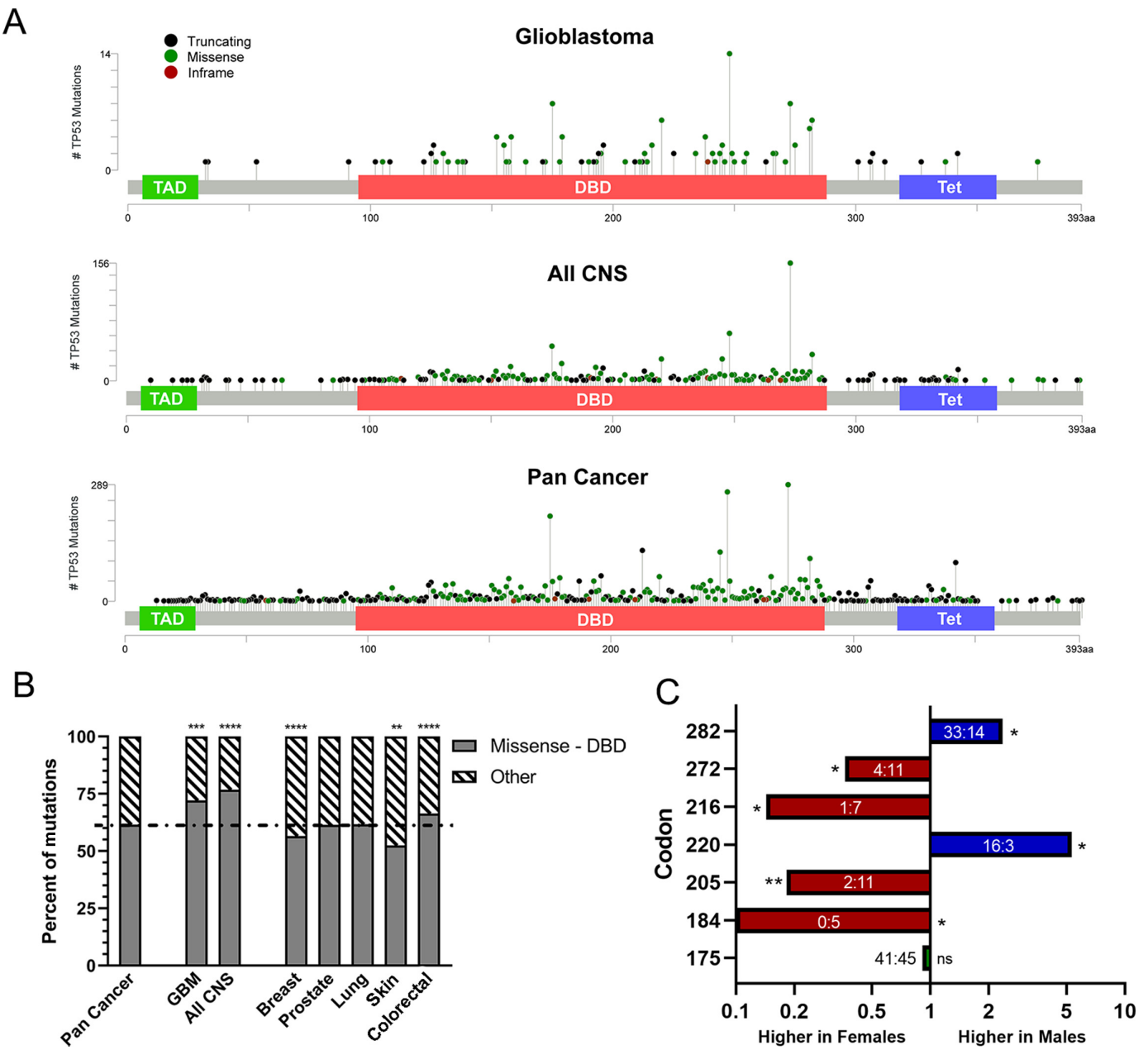

FIGURE 1 p53 missense mutations are enriched in GBM and show a sex difference in incidence. **A,** *TP53* mutation analysis from cBioPortal representing distribution of all truncating, missense, and in-frame *TP53* mutations in glioblastoma, all CNS tumors, and pan-cancer analysis. **B,** The fraction of mutant *TP53* tumors with missense mutations in the DBD (Missense – DBD) was compared with all other *TP53* mutation types and *TP53* domains (Other) in pan-cancer, GBM, CNS tumors, breast cancer, prostate cancer, lung cancer, skin cancer, and colorectal cancer. Significant enrichment or reduction compared with the pan cancer data set was determined by Fisher exact test. **C,** Analysis of the male to female ratio of *TP53* missense mutations in GBM from TCGA, COSMIC, and IARC databases revealed six codons with a significant difference in the frequency of mutations in males and females. Bars are the ratio of male to female tumors with p53 mutated at each codon. The absolute mutation counts are labeled within each bar. Significance was determined by Fisher exact test. *, $P < 0.05$; **, $P < 0.01$; ***, $P < 0.001$; ****, $P < 0.0001$.

We next asked whether the frequency of individual mutations is influenced by patient sex. *TP53* mutation data was combined and analyzed from GBM and CNS tumor specimens from The Cancer Genome Atlas (TCGA), the Catalogue of Somatic Mutations in Cancer (COSMIC), and the International Association for Research on Cancer (IARC) p53 database to determine the frequency of mutations at each codon in the DBD (34–36). In total, 554 male tumors and 442 female tumors were included in the analysis. Six codons, present in 10.8% of all cases were identified as having a sex difference in their mutation frequency by Fisher exact test $P < 0.05$ (Fig. 1C). Four codons were mutated more frequently in females: D184, Y205, V216, and V272, and two codons more frequently in males: Y220 and R282. Notably, both codons more commonly mutated in males are classified as hotspot mutations for their high mutation

frequency across cancers (37). Codon R175 is among the best characterized hotspot mutations and has no sex difference in mutation frequency in GBM. The prevailing hypothesis for pan-cancer hotspot mutations is that these p53 GOF mutations confer a fitness advantage that drives their selection. Applying this same principle to our findings, we hypothesized that that p53 missense mutations have differential GOF effects in males and females that contribute to the selective advantage of certain mutations.

Modeling Mutant p53 GOF

To determine whether there are sex differences in p53 GOF activity, we developed a model of mutant p53 overexpression in mouse primary astrocytes. Briefly, astrocytes were harvested as previously described from the cortices of postnatal day one mouse pups harboring one p53 allele with flanking loxP sites and one deleted p53 allele (14). The pups were sex-typed using the X- and Y-chromosome paralogs, *Jarid1C/D*. Astrocytes from a minimum of three pups were combined per sex to produce male and female $Trp53^{f/-}$ (p53 WT) astrocytes (Fig. 2A; ref. 14). Astrocyte purity was assessed using glial fibrillary acidic protein (GFAP) immunofluorescence (IF; Fig. 2B). To evaluate potential sex differences in p53 GOF, we selected three mutations: $Trp53^{R172H}$, $Trp53^{Y202C}$, and $Trp53^{Y217C}$ for evaluation. $Trp53^{R172H}$ (Hs $TP53^{R175H}$) is among the most common mutations across cancer and has established GOF (17). It exhibits no sex difference in frequency in GBM. $Trp53^{Y202C}$ (Hs $TP53^{Y205C}$) is the mutation with the most significant sex difference in frequency in female patients. $Trp53^{Y217C}$ (Hs $TP53^{Y220C}$) has the most significant sex difference in frequency among the mutations more common in males. Male and female p53 WT astrocytes were transduced with retrovirus to stably overexpress mutant *Trp53*-IRES-*eGFP* for each missense mutation, and eGFP-positive cells were sorted by flow cytometry. A common cooccurring event in cancers expressing mutant p53 is the loss of the second wild-type p53 allele, known as loss-of-heterozygosity (LOH). LOH has been shown to be required for stabilized mutant expression and GOF activity in some mutants (38). To mirror these events in our *in vitro* cell model, WT and mutant p53 astrocytes were transduced with a lentiviral vector expressing Cre recombinase and Puromycin N-acetyl transferase (*Pac*). The cultures were selected for Cre/Pac-positive cells for one week with 2.5 μmol/L puromycin to produce p53 KO and $p53^{mutant/-}$ astrocytes (Fig. 2C). Figure 2D displays a representative Western blot measuring p53 protein levels in each cell line. Under low stress conditions, WTp53 is negatively regulated by the E3 ubiquitin ligase Mdm2. In response to DNA damage, p53 is phosphorylated inhibiting Mdm2 interactions and stabilizing the p53 protein. As a positive control, $p53^{f/-}$ astrocytes were treated with a combination of the DNA-damaging agent etoposide (10 μg/mL) and the Mdm2 inhibitor Nutlin-3a (10 μmol/L) or DMSO for 8 hours leading to stable induction of p53 protein. p53 KO astrocytes expressing Cre but lacking mutant p53 expression had no detectable p53. In contrast, high levels of overexpressed mutant p53 protein were observed in male and female astrocytes transduced with each of the retrovirus-encoded p53 mutations. To confirm the loss of the WT floxed p53 allele in Cre-positive cells, we performed a PCR with primers specific to the floxed and deleted p53 alleles (Fig. 2E). Introduction of Cre eliminated the floxed allele band indicating the complete loss of p53 at the WT locus. To ensure that WTp53 was completely depleted in the Cre-expressing astrocytes, WTp53 and p53KO astrocytes were treated with etoposide and Nutlin-3a or DMSO for 8 hours and p53 protein was detected by IF. Cotreatment induced high levels of nuclear localized p53 in WT astrocytes but resulted in no detectable p53 in the p53 KO astrocytes (Fig. 2F). IF for p53 in male and female astrocytes expressing mutant p53 confirmed that in the absence of treatment all three mutations expressed high levels p53 protein throughout the cell body (Fig. 2G).

Sex Differences in p53 GOF Phenotype

Accelerated proliferation is among the most frequently observed phenotypes attributed to mutant p53 GOF. In addition to the loss of WTp53 regulation of cell cycle, GOF-mutant p53 interacts with several transcription factors to increase the transcription of pro-proliferation genes (17). Thus, we measured the growth effects of each mutation in both sexes. 3,000 male or female p53 WT, p53 KO, $p53^{R172H}$, $p53^{Y202C}$, and $p53^{Y217C}$ astrocytes were plated in triplicate on 10-cm dishes, in three independent experiments, and allowed to expand for eight days before fixing and Giemsa staining nuclei. KO alone increased astrocyte proliferation compared with WT astrocytes but exhibited no detectable sex differences. All three p53 mutations exhibited a GOF growth phenotype in a sex-dependent manner. Expression of $p53^{R172H}$ in females and $p53^{Y202C}$ and $p53^{Y217C}$ in males significantly increased growth in comparison with p53 KO astrocytes and astrocytes expressing the same mutation in the opposite sex (two-way ANOVA, $P < 0.05$). While $p53^{R172H}$ in males, $p53^{Y202C}$ in females, and $p53^{Y217C}$ females were insufficient to increase proliferation over p53 KO (Fig. 3A–C), male $p53^{R172H}$ and female $p53^{Y202C}$ astrocytes formed denser colonies compared with KO, suggesting that these mutations may possess sex-dependent GOF activity (Fig. 3B). In female cells, $p53^{Y217C}$ expression appeared to decrease the growth phenotype compared with KO. To ensure that this effect was not a technical artifact of the assay, we plated a 5-fold titration of male and female p53 KO and $p53^{Y217C}$ astrocytes and incubated them for five days at which point the fastest growing cells reached overconfluency (Supplementary Fig. S1). This experiment confirmed the previous observation, with female $p53^{Y217C}$ growing slower than p53KO, p53KO exhibiting no sex difference, and male $p53^{Y217C}$ growing the fastest. Together, these data support that p53 GOF effects are dependent on an interaction between sex and mutation. Modeling the interaction between sex and mutation as a function of growth revealed a statistically significant interaction between sex and genotype for each mutation (mixed effect linear regression with variances controlled among technical replicates, $p53^{R172H}$ $P = 7.78 \times 10^{-5}$, $p53^{Y202C}$ $P = 0.00413$, $p53^{Y217C}$ $P = 1.41 \times 10^{-8}$).

Next, we asked whether the growth phenotypes were correlated with sex differences in tumorigenicity. Equal numbers of each male and female KO and p53-mutant astrocyte lines were injected into parallel flanks of three male and three female NCr nude mice ($n = 6$) as illustrated in Fig. 3D. Flank tumor volume was measured by digital caliper weekly until the first tumor reached terminal size. Male $p53^{Y217}$, male $p53^{Y202C}$, and female $p53^{R172H}$ tumors grew significantly faster than p53 KO tumors (two-way ANOVA, $P < 0.05$; Fig. 3E). When comparing between sexes, male $p53^{Y217C}$ and female $p53^{R172H}$ tumors grew significantly faster than the same mutation in the opposite sex, while the effects of neither $p53^{Y202C}$ nor p53 KO were significantly affected by sex (Fig. 3E inset, two-way ANOVA, $P < 0.05$). In total, 0/6 KO, 16.7% (1/6) of male and 83.3% (5/6) of female $p53^{R172H}$, 66.6% (4/6) of male and 50% (3/6) of female $p53^{Y202C}$, and 100% (6/6) of male and 16.6% (1/6) of female $p53^{Y217C}$ astrocyte injections formed tumors. In addition to the frequency of tumor formation, female $p53^{R172H}$, male $p53^{Y202C}$, and male $p53^{Y217C}$ tumors were significantly larger than tumors expressing the same mutation in the opposite sex (Fig. 3F, Supplementary Fig. S2, log-transformed Welch-corrected two-tailed t test, $P < 0.05$). When no tumor was recovered, the final tumor volume reflects the volume of the recovered Matrigel pellet. The sex of the host mouse had no observed effect on tumor size or frequency which is consistent with cell-intrinsic

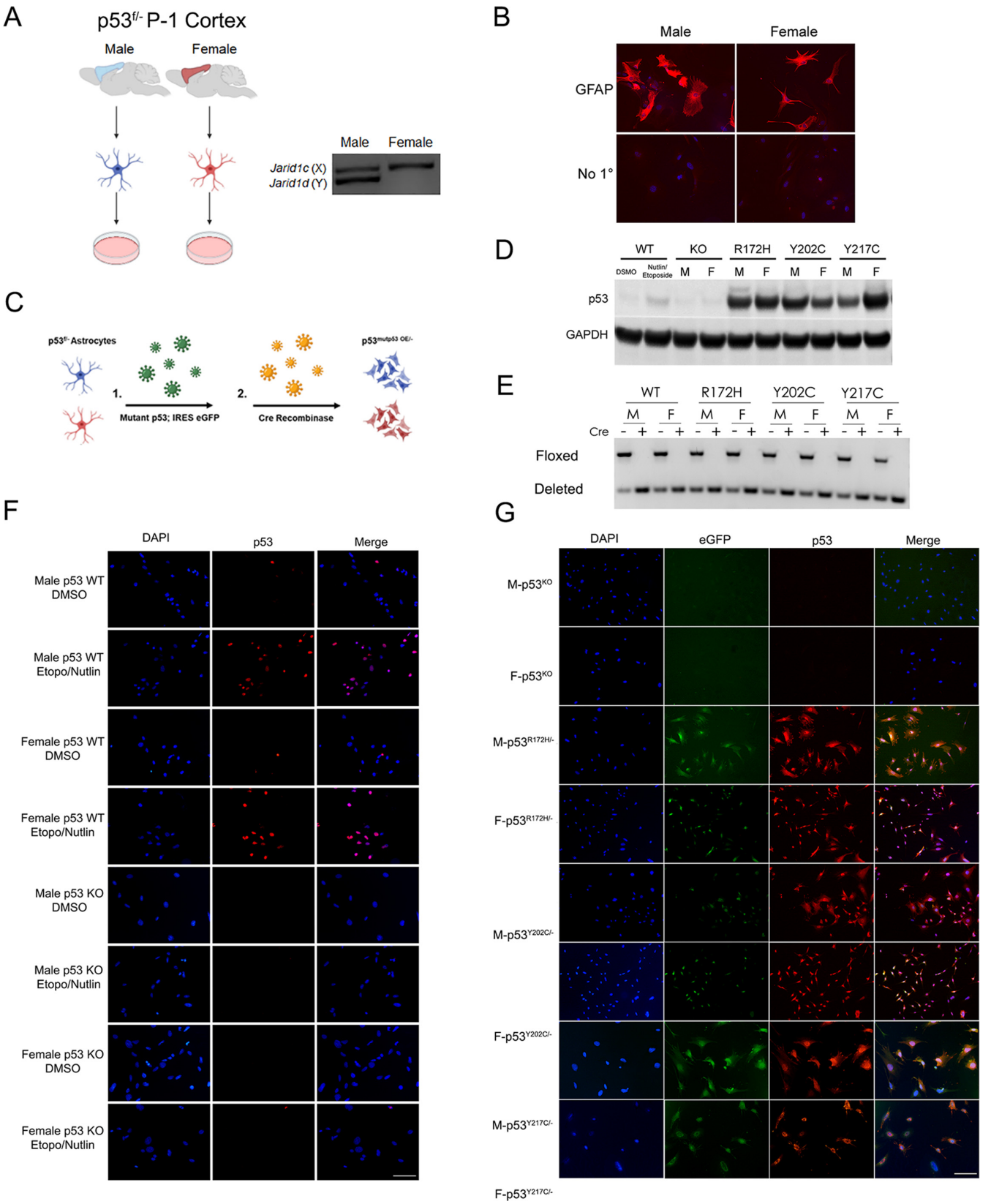

FIGURE 2 Modeling p53 missense mutations in GBM. **A,** *Trp53*$^{f/-}$ astrocytes were isolated from the cortices of male and female postnatal day 1 mouse pups. The sex of the astrocytes was determined by genotyping PCR (left), and male or female astrocytes from at least 3 pups were combined. **B,** Astrocytes were stained for the astrocyte lineage marker GFAP to confirm astrocyte purity. Scale bar, 100 μm. (*Continued on the following page.*)

(*Continued*) **C,** To create mutant p53–expressing astrocytes, *Trp53*$^{f/-}$ astrocytes were transduced with retrovirus to overexpress mutant *Trp53*-IRES-eGFP, and eGFP-positive cells were sorted by flow cytometry. Sorted eGFP-positive astrocytes were transduced with lentivirus to express Cre-IRES-Puro and selected with 2.5 μg/mL puromycin for 1 week. **D,** Western blot assay was performed using 50 μg of whole-cell lysates from male and female *Trp53*$^{f/-}$ (WT), *Trp53* KO, and *Trp53*$^{mut/-}$ astrocytes. *Trp53*$^{f/-}$ (WT) astrocytes were treated with 20 μg/mL etoposide and 10 μg/mL Nutlin-3a or DMSO control for 8 hours. Mutant p53 astrocytes stably express mutant p53 protein at high levels compared without the treatment needed to stabilize WT p53 protein. **E,** Loss of the lox-p53-lox (floxed) allele following introduction of Cre recombinase was confirmed by PCR. **F,** Treatment with Nutlin-3a and etoposide to stabilize p53 results in detectable p53 protein in p53 WT but not p53 KO astrocytes. *Trp53*$^{f/-}$ astrocytes were treated with 20 μg/mL etoposide and 10 μg/mL Nutlin-3a or DMSO for 8 hours and were fixed and stained by IF for p53 protein. Scale bar, 200 μm **G,** IF for GFP (green) and p53 (red) p53 KO and mutant astrocytes. Scale bar, 200 μm.

sex differences as we previously observed (14, 15). Resected tumors all had features indicative of gliomas including nuclear atypia and hypercellularity (Fig. 3G) and expressed high levels of mutant p53 protein (Fig. 3H). In comparison with p53 KO, all mutations exhibited a GOF in tumorigenicity compared with p53 loss regardless of sex. However, three distinct patterns of sex differences in GOF were observed. p53^{R172H} mutants had the greatest female sex effect. p53^{Y202C} had a trend toward greater tumorigenicity in males but had the smallest differences between sexes. p53^{Y217C} GOF activity was greatest in males and was the only mutation which formed tumors from every injection supporting male-specific GOF for this mutation.

Mutant p53 and Genomic Instability

All mutations were introduced at the same astrocyte passage under equivalent conditions with WTp53 intact. Introduction of mutant p53 and loss of WT p53 function disrupts DNA repair and cell-cycle checkpoints leading to genomic instability and the acquisition of additional mutations (39). We questioned whether the observed sex differences in growth and tumorigenicity might be driven by differences in genomic instability or acquisition of sporadic oncogenic mutations. We performed whole-exome sequencing and measured mutational burden in male and female mutant p53–expressing cells and p53 KO cells. Loss of WT p53 function led to equivalently large increases in mutational burden in all eight cell lines. To determine whether overall mutational burden was impacting phenotype, the raw mutation count was plotted against the percent area from the growth assay in Fig. 2. There was no significant correlation between mutational burden and proliferation (Supplementary Fig. S3A). Most mutations identified were silent or intergenic. Further analysis of missense, frame-shift, and nonsense mutations predicted to have a moderate-to-high impact on gene expression or function, also exhibited similar frequencies between cell lines with no correlation between the number of mutations and growth (Supplementary Fig. S3B).

Finally, we asked whether there were any unique mutations that could be contributing to these phenotypic differences. Supplemental Table S2 lists every gene with a homozygous missense, frame-shift, or nonsense mutation in at least one cell line. Almost all mutated genes were altered across tumor-forming and non-tumor–forming cells. Three genes, *Calcoco2*, *Rbmy*, and *Thap1* were identified as uniquely mutated only in male p53^{Y202C} cells. None of these genes have been described as cancer-related. Together, these data suggest that genomic instability and the acquisition of sporadic mutations does not account for the observed sex differences.

P53 Mutants Drive Unique Transcriptional Programs in Males and Females

One of the primary mechanisms of mutant p53 GOF activity is the transcriptional regulation of genes in protumorigenic pathways. Previous studies have identified several oncogenic targets of both R175H and Y220C mutations (17). To determine whether mutant p53 exhibits GOF transcriptional activity, we performed mRNA-sequencing (RNA-seq) on RNA isolated from each cell line and compared the differentially expressed genes between each mutation and p53 KO within each sex. In all cases, introduction of mutant p53 led to significant changes in gene expression compared with p53 KO, confirming neomorphic transcriptional function (FDR < 0.05; Supplementary Fig. S4). We next compared the differentially expressed genes between male and female astrocytes within each mutation. p53 KO, p53^{R172H}, p53^{Y202C}, and p53^{Y217C} yielded 7183, 9013, 10,902, and 10,748 significant differentially expressed genes between sexes, respectively (FDR < 0.05; Fig. 4A). Predictably, sex chromosome–linked genes including the X-linked genes *Xist, Agtr2*, and *Eda*, and the Y-linked genes *Uty, Eif2s3y, Ddx3y,* and *Kdm5d* are among the most differentially expressed genes across all mutations. However, these genes represent only a small fraction of the genes with a sex difference in expression.

To evaluate how gene expression varies as a function of p53 mutation and sex, we performed a sparse principal component analysis. The first three principal components account for 75.8% of total variance. Strikingly, the samples clustered primarily by their ability to form tumors with low-tumorigenic male and female KO, male p53^{R172H}, and female p53^{Y217C} clustering together, while high-tumorigenic female p53^{R172H}, female p53^{Y202C}, male p53^{Y202C}, and male p53^{Y217C} clustered independently (Fig. 4B; Supplementary Fig. S5). Among the cell lines with high tumorigenic potential, the first two principal components account for the majority of sex differences with male p53^{Y202C} and p53^{Y217C} separating in PC1 and female p53^{Y202C} and p53^{R172H} separating in PC2. Meanwhile, PC3 encompasses the majority of variation between mutants. The normalized expression for all genes contributing to each principal component are displayed in heat maps in Fig. 4C. All tumor-forming cell lines have distinct transcriptomes, suggesting that neither sex nor p53 mutation status alone explain the variation in gene expression. Rather, it is the interaction between mutation and sex that drives unique transcriptional phenotypes.

Sex and Mutant p53 Interact in the Regulation of Oncogenic Pathways

To characterize the sex-specific GOF transcriptome of each mutation, differentially expressed genes between mutant p53 and p53 KO were compared between sexes to define the sex specific (unique) and shared (overlapping) transcriptional impact of each mutation. We focused our analysis on those genes with an absolute $\log_2$ fold change greater than 0.5. KEGG pathway enrichment analysis was used to evaluate whether shared or sex-specific changes in gene expression could be contributing to the differing tumorigenic phenotypes. Concordant with differences in tumorigenesis, pathway analysis revealed three independent transcriptional patterns. p53^{R172H} expression had a substantially greater impact in females than males with approximately 7.4× more female-specific

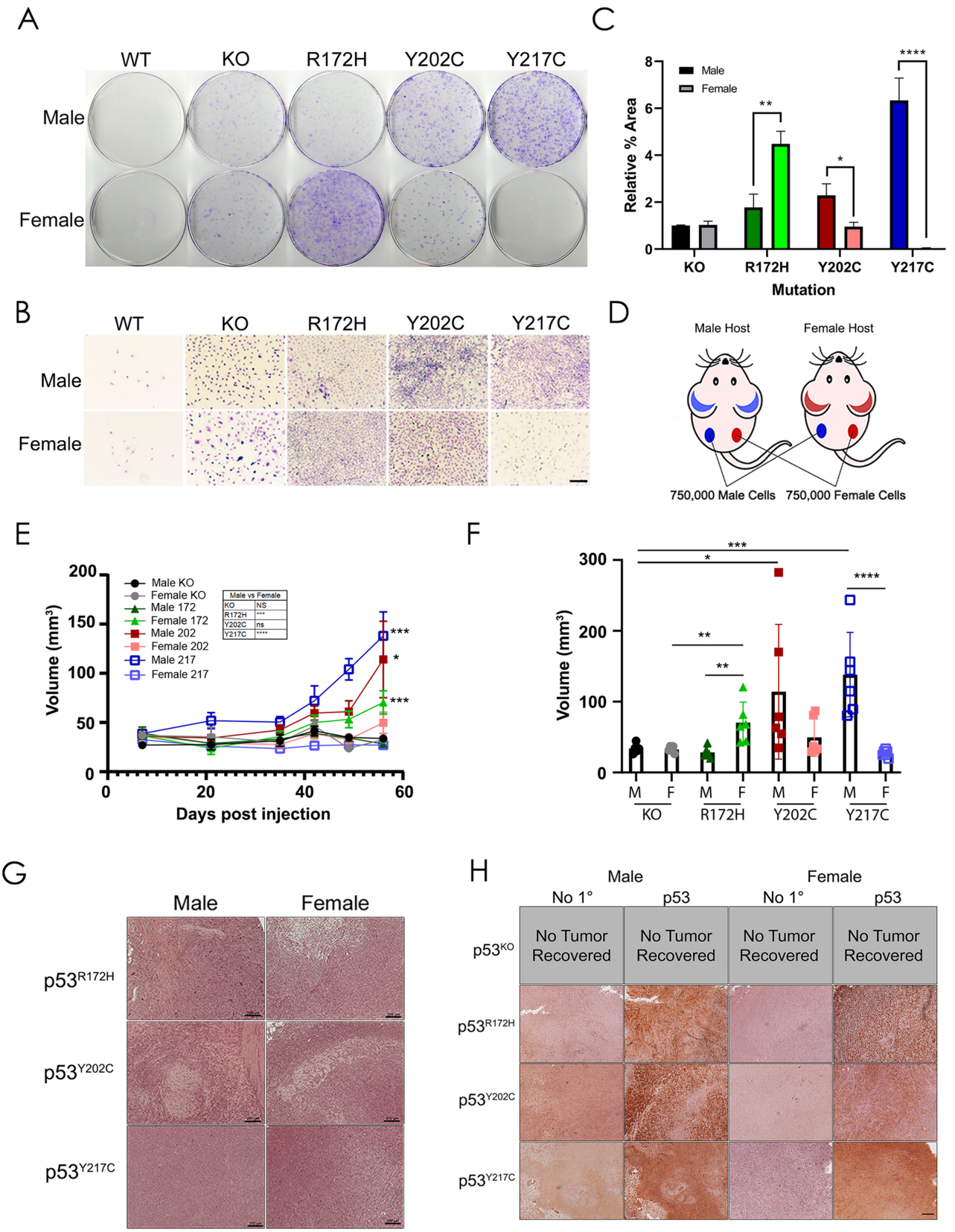

FIGURE 3 p53 missense mutations exhibit sex-specific GOF effects on growth and tumorigenicity. **A,** Male and female WT p53, p53 KO, $p53^{R172H}$, $p53^{Y202C}$, and $p53^{Y217C}$ astrocytes were plated at 3,000 cells per 10 cm and incubated in normal growth conditions for 8 days, fixed with 100% methanol, and stained with Giemsa stain. Representative plates show a sex-specific GOF growth phenotype. (*Continued on the following page.*)

(*Continued*) **B,** Representative magnified images of astrocyte colonies showing differences in the density of colonies between male and female mutant p53 astrocytes. Scale bar, 100 μm. **C,** The percent area covered by stained cells was quantified in ImageJ and normalized to male KO controls ($n = 3$). Significance determined by unpaired Student *t* test. **D,** Schematic of subcutaneous flank injection protocol. 750,000 male and female astrocytes were injected subcutaneously into the opposing flanks of 3 male and 3 female nude mice. **E,** Flank tumors were measured weekly using a digital caliper ($n = 6$). Female $p53^{R172H}$, male $p53^{Y202C}$, and male $p53^{Y217C}$ tumors grew significantly faster than their sex-matched p53 KO astrocytes. $p53^{R172H}$ and $p53^{Y217C}$ tumors also exhibited sex differences in tumor growth (inset table). Significance was determined by two-way ANOVA. **F,** Tumors were harvested from the mouse flanks and volumes measured postresection. When no tumor was recovered, the original Matrigel injection was measured for final tumor volume. Significant differences in tumor volume were determined by performing a log-transformed Welch-corrected two-tailed *t* test. **G,** Representative hematoxylin and eosin–stained sections from flank tumors. Scale bars, 200 μm. **H,** IHC staining was performed on each resected tumor showing high expression of mutant p53 in the tumor. Scale bar, 200 μm. *, $P < 0.05$; **, $P < 0.01$; ***, $P < 0.001$; ***, $P < 0.0001$.

differentially expressed genes (Fig. 5A). Pathway analysis revealed that shared differentially expressed genes were enriched for KEGG cancer pathways. In addition, shared genes were enriched for many cancer-associated pathways including cell cycle, DNA replication, p53 signaling, focal adhesion, senescence, and Rap1 signaling. The genes differentially expressed uniquely in males were not enriched for any cancer-associated pathways. Meanwhile, genes that were differentially expressed in females alone were also enriched for many KEGG cancer pathways and cancer-associated pathways including extracellular matrix receptor signaling, stem cell pluripotency, and PI3K–Akt signaling among others. This indicates that $p53^{R172H}$ has both female-specific and sex-independent GOF effects on gene expression in cancer-relevant pathways, and the combined effect is sufficient for tumorigenesis in females, while the shared GOF alone is insufficient in males.

The $p53^{Y202C}$ mutation had the smallest sex difference in GOF phenotype with both males and females forming large tumors *in vivo*, and the smallest differences in sex-specific genes of any mutation. For this mutation, the overlapping gene list was enriched for cancer pathways and cancer-associated pathways with very few enriched pathways in the sex-specific differentially expressed genes (Fig. 5B). Together, this reveals a second GOF transcriptional profile in which the shared GOF activity is sufficient for transformation in both sexes with very little sex-specific effect on transformation.

The $p53^{Y217C}$ mutation represents a third interaction between mutation and sex (Fig. 5C). Here, male-specific genes were the only subset enriched for KEGG cancer pathways, with very little pathway enrichment in the shared or female component. Male-specific genes were enriched for pathways in cancer, Rap1

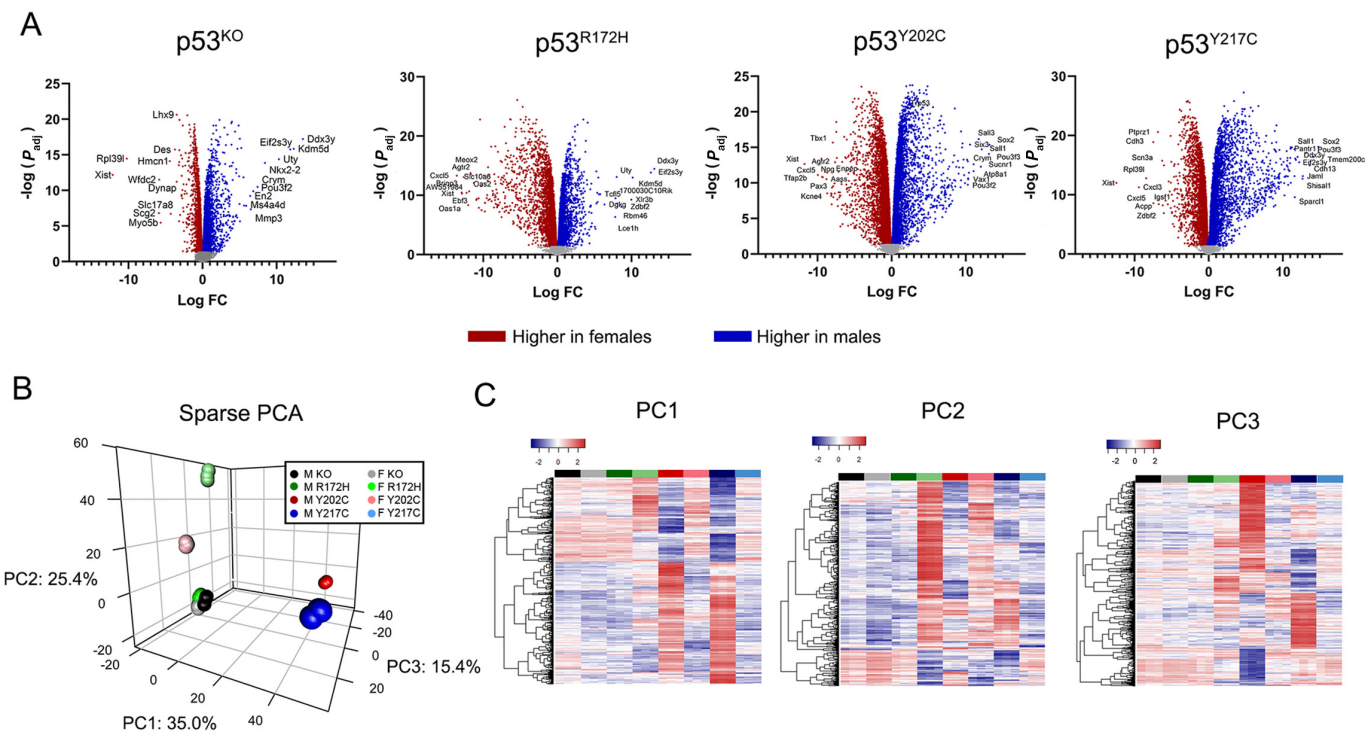

FIGURE 4 p53 missense mutations have sex-specific/mutation-specific GOF effects on gene expression. **A,** Volcano plots of all significant differentially expressed genes between males (blue) and females (red). The labeled points represent the ten genes with the greatest differences in expression (logFC). Significance was determined by FDR < 0.05. **B,** Sparse PCA analysis displaying variation between highly tumorigenic and weakly tumorigenic cell lines. **C,** Heat maps with hierarchical clustering of $\log_2$-transformed CPM for all genes contributing to each principal component in the sparse PCA analysis. Each colored bar spans three independent replicates for each mutation in each sex. Colors matched the figure legend in **B**.

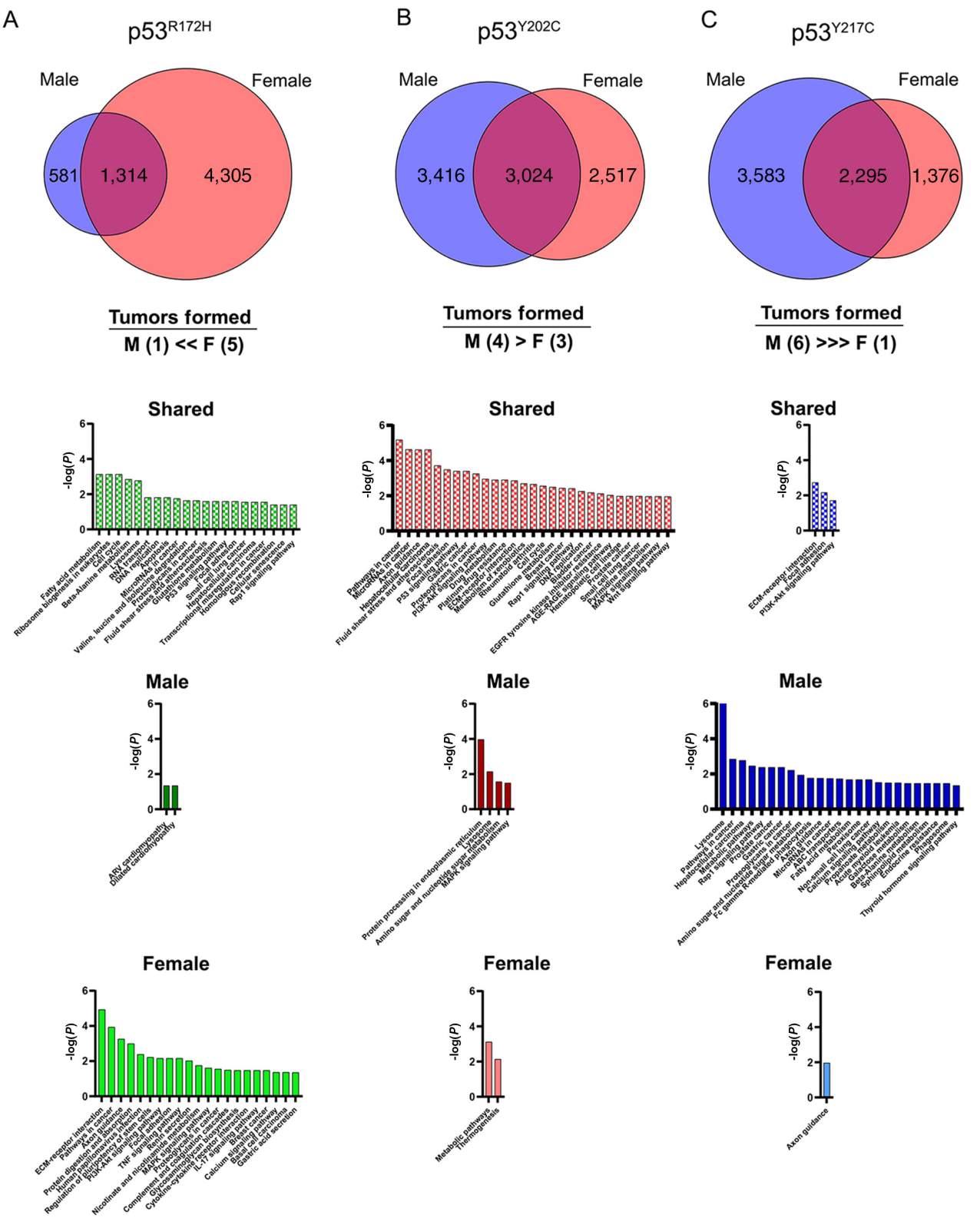

FIGURE 5 Sex and mutation interact to drive gene expression patterns in cancer pathways concordant with the tumorigenic phenotype. All differentially expressed genes (log fold change; logFC > 0.5, FDR < 0.05) between each mutation and p53 KO were compared to define the sex-specific and shared GOF transcriptional profile. Venn diagrams display the number of shared and sex-specific differentially expressed genes. KEGG pathway enrichment analysis (FDR < 0.05) applied to each corresponding gene list revealed sex- and mutation-specific patterns of enrichment for changes in cancer-associated pathways (orange) for $p53^{R172H}$ (**A**), $p53^{Y202C}$ (**B**), and $p53^{Y217C}$ (**C**). The magnitude of sex difference in GOF phenotype (number of tumors formed *in vivo*) is displayed below each Venn diagram.

signaling, proteoglycans in cancer, miRNAs in cancer, several tissue-specific cancer pathways, and cancer-associated metabolic pathways. These data support a model in which $p53^{Y217C}$ has male-specific GOF effects on transcription with little universal or female-specific activity in cancer-relevant pathways.

To further interrogate the interaction between sex and mutation, we modeled the changes in gene expression for all genes as a function of sex and mutation. We identified 9,287, 10,441, and 9,387 genes for $p53^{R172H}$, $p53^{Y202C}$, and $p53^{Y217C}$, respectively with a significant interaction between sex and mutation (FDR < 0.05). Importantly, this analysis is highly concordant with the gene sets assembled by differential expression analysis above (Supplementary Table S3). Subsequent pathway enrichment analysis of the gene overlapping between both analyses revealed similar KEGG pathways to those identified in the differential expression analysis alone (Supplementary Tables S4–S6). Modeling the interaction of mutation and gene expression independent of sex also revealed a higher degree of concordance (99%) with the shared differentially expressed gene lists (Supplementary Table S7). Together, these analyses support that cell sex and p53 mutations interact to drive unique transcriptional programs.

Sex Differences in Mutant p53 GOF Activity Is Mediated Through Differential Genomic Localization

Having established that mutant p53 expression leads to unique GOF transcriptional profiles dependent on both mutation and sex, we next sought to determine the mechanism underlying mutant p53 transcriptional regulation. We performed chromatin immunoprecipitation with massively parallel DNA sequencing (ChIP-seq) to map mutant p53 localization. To understand the sex differences in mutant p53 function, we focused on the mutation with the greatest female-specific effect, $p53^{R172H}$, and greatest male-specific effect, $p53^{Y217C}$. Regions enriched for mutant p53 localization were then mapped relative to their distance from the transcriptional start sites (TSS) of the top 1000 upregulated genes for each mutation in males and female (Fig. 6A). In both males and females, $p53^{R172H}$ localization was enriched near the TSSs of a subset of upregulated genes indicating that mutant p53 directly regulates aberrant gene expression in both sexes. In $p53^{Y217C}$ cells, localization was enriched at TSSs of upregulated genes in males but displayed no pattern of localization in females.

Previous studies have established that mutant p53 lacks a consensus binding sequence, but instead relies on interactions with other transcription factors and DNA-binding proteins for localization to aberrant target genes. To identify potential mediators of mutant p53 activity, we performed a HOMER analysis on the enriched ChIP signals ± 5 kb of the TSS of the same 1,000 upregulated genes enriched for p53 localization. The top five significant known motifs identified in male and female $p53^{R172H}$ and male $p53^{Y217C}$ are presented in Fig. 6B. In all three analyses, mutant p53 was found to localize to the consensus sequence of a unique set of transcription factors, suggesting that the sex-specific GOF activity of each mutation may be driven by different sets of transcriptional mediators.

The transcription factor AP-2gamma (*TFAP2C*) is a known regulator of stem cell self-renewal and chemotherapy resistance (40). We found that in females but not males $p53^{R172H}$ localization is enriched at AP-2gamma DNA-binding motifs. *WNT5A* has been shown to be upregulated in glioma and is associated with poor overall survival (41). In our model, *Wnt5a* mRNA was significantly upregulated in female $p53^{R172H}$ and downregulated in male $p53^{R172H}$. This difference in gene expression is consistent with greater ChIP-seq signal in females compared with males at the AP-2gamma motif near the TSS of *Wnt5a* (Fig. 6C). Similarly, $p53^{Y217C}$ localized to the androgen receptor-half site motif located upstream of the growth factor Fgf2 in males but not females correlating with sex differences in gene expression (Fig. 6D). These results suggest that sex differences in mutant p53 GOF gene regulation may be mediated through differential localization to the consensus sequences of known transcription factors upstream of oncogenes.

Discussion

p53 is the most interrogated protein in cancer research. A PubMed search of p53, *TP53*, and *Trp53* reveals an annual average of 6,000 p53 publications over past five years. Despite this herculean effort, our understanding of the most mutated gene in cancer remains incomplete. An obstacle to fully characterizing WT and mutant p53 activity is its context dependence in function. WT p53 is positioned at the center of a complex network of cellular pathways whose precise activation profile is determined by cell identity and the stimulus activating the p53 response (1). Similarly, p53 mutations result in a spectrum of cancer phenotypes dictated by the tumor type, cooccurring mutations, and specific p53 mutation (19). Mounting evidence in both normal development and disease support that sex is a key modulator of p53 function, and that a full understanding of WT and mutant p53 will require incorporating the scope and magnitude of these sex effects.

Most mutations in tumor suppressors prevent gene expression or protein production or result in an unstable protein that is quickly degraded. In contrast, p53 GOF activity selects for stable expression of mutant p53 protein over loss-of-function mutations or deletions. However, the importance p53 GOF mutations is rarely reflected in *in vitro* and mouse cancer models that more frequently rely on dominant negative p53 constructs, or p53 knockdown or deletion. In GBM, complete p53 loss is an uncommon event. Our analysis of p53-mutant tumors revealed that missense mutations in the DBD are particularly enriched in GBM and CNS cancers compared with other cancers. Together, with previous studies of LFS demonstrating an association between germline DBD mutations and a higher risk of brain tumor development, these findings support a CNS tissue–specific advantage of p53 GOF mutation in tumor development (32). This finding also suggests the fidelity of GBM models could be enhanced by inclusion of clinically relevant p53 GOF mutations.

In this study, we revealed a novel interaction between p53 mutation and cell sex. We found that while p53 deletion increased proliferation, it is insufficient to transform astrocytes and does not induce a sex difference in phenotype. In contrast, introduction of GOF mutant p53 into the same cells was sufficient for transformation, with the magnitude of tumorigenic potential dependent on the mutation and cell sex. The hotspot mutation $p53^{Y217C}$ exhibited the greatest GOF and greatest sex difference of all three tested mutations. Male $p53^{Y217C}$ cells were highly proliferative and tumorigenic while female $p53^{Y217C}$ cells exhibited no GOF phenotype compared with KO. Notably, this relationship is concordant with a greater mutation frequency of $p53^{Y220C}$ in human males. $p53^{R172H}$ exhibited the opposite effect with the GOF effect predominant in females with little impact on tumorigenesis in males. In humans, this mutation was found in equal prevalence in both sexes. Independent of p53 status, GBM is more common in males than females (incidence ratio of 1.6:1; ref. 42). If a mutation were to have equal GOF effects in both sexes, we would expect it to present at a similar incidence ratio to GBM overall. A potential explanation for the lack of sex difference in the incidence of $p53^{R175H}$ is that the female-specific GOF activity compensates for the other factors that would otherwise result in a greater incidence in males. The third mutation, $p53^{Y202C}$, had the smallest sex difference in GOF. While males grew faster *in vitro*, both males and females formed tumors

A

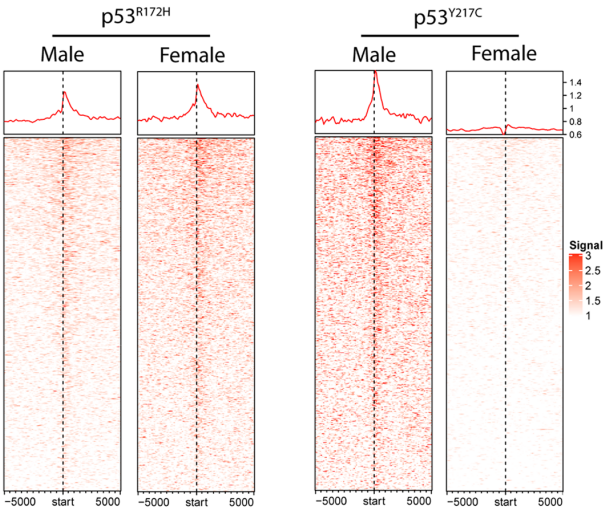

B

Male p53^{R172H}

Consensus Sequence	Motif Name	Description	*P*
	JunD	JunD Proto-Oncogene	0.00001
	ZNF165	Zinc Finger Protein 165	0.0001
	Atf2	Activating Transcription Factor 2	0.0001
	c-Jun-CRE	c-Jun ChIP-Seq Motif	0.0001
	Atf7	Activating Transcription Factor 7	0.001

Female p53^{R172H}

Consensus Sequence	Motif Name	Description	*P*
	GRE	Glucocorticoid Response Element	0.001
	AP-2gamma	Activating Enhancer-Binding Protein 2 Gamma	0.001
	RUNX	RUNX Family Consensus Sequence	0.01
	E2A	TCF3 E Protein Transcription Factor	0.01
	ARE	Androgen Receptor Response Element	0.01

Male p53^{Y217C}

Consensus Sequence	Motif Name	Description	*P*
	Brn1	POU Class 3 Homeobox 3	0.001
	AR-halfsite	Androgen Receptor Halfsite	0.001
	RAR:RXR	Retinoic Acid/Retinoid X Receptor	0.001
	Rbpj1	Recombination Signal Binding Protein For Immunoglobulin Kappa J Region	0.01
	ZNF189	Zinc Finger Protein 189	0.01

C

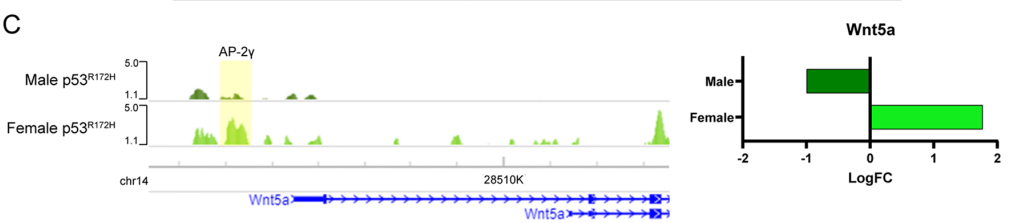

D

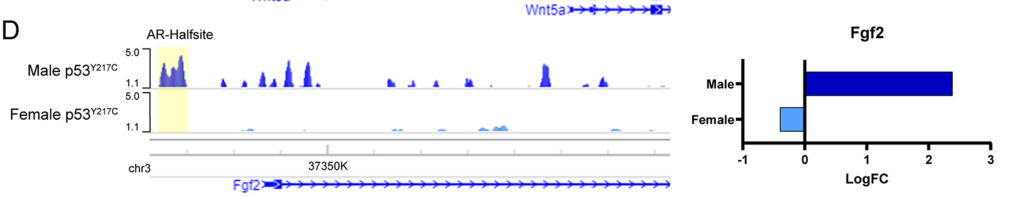

FIGURE 6 ChIP-seq revealed mutant p53 localization at TSSs is enriched for sex/mutation-specific transcription factor DNA-binding motifs. **A,** Heat maps of mutant p53 ChIP-seq enrichment over input ± 5 kb from TSSs of the top 1,000 upregulated genes compared with p53 KO for male and female p53^{R172H} and p53^{Y217C}. The line graph above each heat map displays the average signal across all 1,000 genes. (*Continued on the following page.*)

(*Continued*) **B,** HOMER analysis of $p53^{R172H}$ in males and females and $p53^{Y217C}$ in males within ± 5 kb of the TSSs. The top five significantly enriched known consensus sequences for each mutation and sex are shown. **C,** Female enriched $p53^{R172H}$ localization at the AP-2γ motif (yellow) in the TSS of *Wnt5a* correlates with increased gene expression compared with males. **D,** Male-specific $p53^{Y217C}$ localization at the AR-halfsite motif (yellow) in the TSS of *Fgf2* correlates with increased gene expression compared with females. Bar graphs display the logFC in gene expression between each mutation and p53 KO with the same sex.

in vivo. In this instance, the cell-intrinsic sex effect is not concordant with the observed greater incidence in human females. The lack of concordance suggests additional factors involving such mechanisms as cell:cell interactions within the tumor microenvironment or systemic effects of immunity or metabolism, likely supersede the cell-intrinsic, sex-specific GOF effect of this mutation. In contrast, sex differences in $p53^{Y217C}$ GOF activity appear to be a dominant effector of sex differences in tumorigenicity. The differences in concordance between the laboratory and clinical phenotypes of these mutants may provide an important tool for investigating the mechanisms by which cell-intrinsic effects of p53 mutations interact with tissue- and systems-level factors to determine cancer phenotypes.

Mutant p53 promotes tumorigenesis through the aberrant regulation of oncogenic target genes. Using RNA-seq, we characterized a sex-specific and sex-independent GOF transcriptional profile – defined as the differential gene expression between mutant p53 and p53 KO – for each missense mutation. All three mutations resulted in sex- and mutation-specific gene expression patterns with thousands of differentially expressed genes. Comparing the GOF transcriptional profiles between sexes revealed three distinct gene expression patterns concordant with the tumorigenic phenotypes. In $p53^{Y217C}$, the male GOF profile was enriched for many cancer pathways, with few pathways enriched in the shared or female-specific profiles. This male-specific GOF transcriptional profile is consistent with the male-specific GOF phenotype. $p53^{R172H}$, which had the greatest female-specific GOF phenotype, exhibited enrichment for cancer-relevant pathways in both the female specific and shared differentially expressed genes, and no enrichment for cancer pathways in males. This points to a second model where $p53^{R172H}$ acts on a set of female-specific and sex-independent target genes whose effects interact to drive sex differences in tumor formation. In the third scenario, $p53^{Y202C}$ was only enriched for cancer pathways in the shared component indicating the GOF activity enacted by this mutation is sex independent, which is consistent with the similar rates of tumor formation that we observed in these cells. These findings indicate that mutant p53 can have both sex-dependent and sex-independent GOF activity, and that the impact of each on tumorigenesis is mutation specific.

Lopes-Ramos and colleagues recently demonstrated that in normal tissues, transcription factors that are not differentially expressed between males and females have different regulatory binding patterns in males and females (43). The differences in transcription factor binding thus contribute to sex-biased transcriptional programs. In our study, we demonstrated that sex differences in mutant p53 GOF are being driven by differential mutant p53 localization. In both male and female astrocytes, $p53^{R172H}$ localizes to the TSS of a subset of upregulated genes with greater overall enrichment in females. Whereas in $p53^{Y217C}$, we only observed mutant p53 localization at upregulated genes in males with discernable pattern of p53 binding above input in females. This is consistent with a universal- and female-specific GOF by $p53^{R172H}$ and a male-specific GOF by $p53^{Y217C}$.

Mutant p53 lacks a consensus response element and relies on interactions with other transcription factors for localization. By performing HOMER motif enrichment analysis for regions near the TSSs of the top upregulated genes, we identified several novel candidate transcription factors that may be contributing to sex differences in mutant p53 localization and gain of aberrant transcriptional output. Understanding the exact mechanisms of sex-specific mutant p53 localization and gene expression will require the interrogation of each potential binding partner. However, here we highlight two promising potential co-transactivators: female-specific $p53^{R172H}$ enrichment at the AP-2gamma motif upstream of *Wnt5a* and male-specific $p53^{Y217C}$ enrichment at the AR-halfsite motif upstream of *Fgf2*. AP-2gamma is an essential transcription factor for several developmental pathways including neural tube development and male gonad development. It also has been shown to act as an oncogene in breast cancer, melanoma, testicular cancer, neuroblastoma, ovarian cancer, and lung cancer (44). Expression of AP-2gamma is associated with stem cell renewal, proliferation, and therapy resistance (44). *Wnt5a* is upregulated in GBM and has been shown to drive proliferation and invasion in cancer stem cell (CSC) populations (45). Androgen receptor (AR) is known to positively regulate the expression *Fgf2* in prostate cancer (46). In GBM, FGF2 promotes CSC maintenance through interactions with the receptor FGFR1 (47). AR is expressed in both male and female GBM, and androgen receptor antagonists are being evaluated as novel therapeutic strategies (48).

Despite the massive effort to dissect p53 biology, our understanding of this central tumor suppressor remains incomplete. Here, we demonstrated that the same mutations in p53 have unique GOF activity when expressed in otherwise isogenic male and female astrocytes. Our finding highlights sex as a critical determinant of mutant p53 GOF biology. This raises an important question: to what extent has the absence of a consideration of sex limited the approach to investigating p53 function, confounded the interpretation of results, and obscured our understanding of p53 biology? This possibility must be evaluated further as we move forward to improve our understanding of this complex pathway and increase the potential for developing treatments that target the unique effectors of p53 function in male versus female tumors.

Authors' Disclosures

M.V. Staller reports grants from NIGMS and grants from BWF during the conduct of the study. D. Baldridge reports grants from The Children's Discovery Institute of Washington University and St. Louis Children's Hospital during the conduct of the study. No disclosures were reported by the other authors.

Authors' Contributions

N.C. Rockwell: Conceptualization, data curation, formal analysis, investigation, methodology, writing-original draft. **W. Yang:** Formal analysis, writing-review and editing. **N.M. Warrington:** Formal analysis, investigation, writing-review and editing. **M.V. Staller:** Resources, methodology, writing-review and editing. **M. Griffith:** Formal analysis, funding acquisition, writing-review and editing. **O.L. Griffith:** Formal analysis, funding acquisition, writing-review and editing. **C.A. Gurnett:** Funding acquisition, writing-review and editing.

B.A. Cohen: Resources, formal analysis, funding acquisition, writing-review and editing. **D. Baldridge:** Resources, funding acquisition, writing-review and editing. **J.B. Rubin:** Conceptualization, resources, formal analysis, funding acquisition, methodology, writing-review and editing.

Acknowledgments

This work was supported by NIH grant RO1 CA174737-06 (to J.B. Rubin), the Children's Discovery Institute of Washington University and St. Louis Children's Hospital (to M. Griffith, O.L. Griffith, C.A. Gurnett, B.A. Cohen, D. Baldridge, J.B. Rubin), and Joshua's Great Things (to J.B. Rubin). We thank the Alvin J. Siteman Cancer Center at Washington University School of Medicine and Barnes-Jewish Hospital in St. Louis, MO, and the Institute of Clinical and Translational Sciences (ICTS) at Washington University in St. Louis, for the use of the Genome Technology Access Center, which provided RNA-, DNA-, and ChIP-seq services. The Siteman Cancer Center is supported in part by an NCI Cancer Center Support Grant #P30 CA091842 and the ICTS is funded by the NIH's NCATS Clinical and Translational Science Award (CTSA) program grant #UL1 TR002345. We also thank the Alvin J. Siteman Cancer Center at Washington University School of Medicine and Barnes-Jewish Hospital in St. Louis, MO, for the use of the Siteman Flow Cytometry, which provided flow sorting of eGFP-positive cells. We additionally thank Alexia Thia for her technical support including cell culture and *Mycoplasma* testing.

Note

Supplementary data for this article are available at Cancer Research Communications Online (https://aacrjournals.org/cancerrescommun/).

Received August 12, 2021; revised October 28, 2021; accepted December 03, 2021; published first December 15, 2021.

References

1. Kastenhuber ER, Lowe SW. Putting p53 in Context. Cell 2017;170: 1062-78.
2. Olivier M, Hollstein M, Hainaut P. TP53 mutations in human cancers: origins, consequences, and clinical use. Cold Spring Harb Perspect Biol 2010;2: a001008.
3. Laptenko O, Prives C. Transcriptional regulation by p53: one protein, many possibilities. Cell Death Differ 2006;13: 951-61.
4. Li X, Miao X, Wang H, Xu Z, Li B. The tissue dependent interactions between p53 and Bcl-2 *in vivo*. Oncotarget 2015;6: 35699-709.
5. Hafner A, Bulyk ML, Jambhekar A, Lahav G. The multiple mechanisms that regulate p53 activity and cell fate. Nat Rev Mol Cell Biol 2019;20: 199-210.
6. Delbridge ARD, Kueh AJ, Ke F, Zamudio NM, El-Saafin F, Jansz N, et al. Loss of p53 causes stochastic aberrant X-chromosome inactivation and female-specific neural tube defects. Cell Rep 2019;27: 442-54.e5.
7. Kawamata M, Ochiya T. Two distinct knockout approaches highlight a critical role for p53 in rat development. Sci Rep 2012;2: 945.
8. Kim JY, Casaccia-Bonnefil P. Interplay of hormones and p53 in modulating gender dimorphism of subventricular zone cell number. J Neurosci Res 2009;87: 3297-305.
9. Austad SN, Bartke A. Sex differences in longevity and in responses to anti-aging interventions: a mini-review. Gerontology 2015;62: 40-6.
10. Tower J. The genetic architecture of aging: sexual antagonistic pleiotropy of p53 and foxo. Cell Cycle 2010;9: 3840-1.
11. Haupt S, Caramia F, Herschtal A, Soussi T, Lozano G, Chen H, et al. Identification of cancer sex-disparity in the functional integrity of p53 and its X chromosome network. Nat Commun 2019;10: 5385.
12. Gonzalez KD, Noltner KA, Buzin CH, Gu D, Wen-Fong CY, Nguyen VQ, et al. Beyond Li Fraumeni Syndrome: clinical characteristics of families with p53 germline mutations. J Clin Oncol 2009;27: 1250-6.
13. Haupt S, Mitchell C, Corneille V, Shortt J, Fox S, Pandolfi PP, et al. Loss of PML cooperates with mutant p53 to drive more aggressive cancers in a gender-dependent manner. Cell Cycle 2013;12: 1722-31.
14. Sun T, Warrington NM, Luo J, Brooks MD, Dahiya S, Snyder SC, et al. Sexually dimorphic RB inactivation underlies mesenchymal glioblastoma prevalence in males. J Clin Invest 2014;124: 4123-33.
15. Kfoury N, Sun T, Yu K, Rockwell N, Tinkum KL, Qi Z, et al. Cooperative p16 and p21 action protects female astrocytes from transformation. Acta Neuropathol Commun 2018;6: 12.
16. Hainaut P, Pfeifer GP. Somatic TP53 mutations in the era of genome sequencing. Cold Spring Harb Perspect Med 2016;6: a026179.
17. Stein Y, Rotter V, Aloni-Grinstein R. Gain-of-Function mutant p53: all the roads lead to tumorigenesis. Int J Mol Sci 2019;20: 6197.
18. Pfister NT, Prives C. Transcriptional regulation by wild-type and cancer-related mutant forms of p53. Cold Spring Harb Perspect Med 2017;7: a026054.
19. Freed-Pastor WA, Prives C. Mutant p53: one name, many proteins. Genes Dev 2012;26: 1268-86.
20. Rubin JB, Lagas JS, Broestl L, Sponagel J, Rockwell N, Rhee G, et al. Sex differences in cancer mechanisms. Biol Sex Differ 2020;11: 17.
21. Ostrom QT, Rubin JB, Lathia JD, Berens ME, Barnholtz-Sloan JS. Females have the survival advantage in glioblastoma. Neuro Oncol 2018;20: 576-77.
22. Zhang M, Yang D, Gold B. Origin of mutations in genes associated with human glioblastoma multiform cancer: random polymerase errors versus deamination. Heliyon 2019;5: e01265.
23. Dobin A, Davis CA, Schlesinger F, Drenkow J, Zaleski C, Jha S, et al. STAR: ultrafast universal RNA-seq aligner. Bioinformatics 2013;29: 15-21.
24. Liao Y, Smyth GK, Shi W. featureCounts: an efficient general purpose program for assigning sequence reads to genomic features. Bioinformatics 2014;30: 923-30.
25. Patro R, Duggal G, Love MI, Irizarry RA, Kingsford C. Salmon provides fast and bias-aware quantification of transcript expression. Nat Methods 2017;14: 417-19.
26. Wang L, Wang S, Li W. RSeQC: quality control of RNA-seq experiments. Bioinformatics 2012;28: 2184-5.
27. Robinson MD, McCarthy DJ, Smyth GK. edgeR: a Bioconductor package for differential expression analysis of digital gene expression data. Bioinformatics 2010;26: 139-40.
28. Ritchie ME, Phipson B, Wu D, Hu Y, Law CW, Shi W, et al. limma powers differential expression analyses for RNA-sequencing and microarray studies. Nucleic Acids Res 2015;43: e47.
29. Liu R, Holik AZ, Su S, Jansz N, Chen K, Leong HS, et al. Why weight? Modelling sample and observational level variability improves power in RNA-seq analyses. Nucleic Acids Res 2015;43: e97.
30. Erichson N, Zheng P, Manohar K, Brunton S, Kutz J, Aravkin A. Sparse principal component analysis via variable projection. SIAM J Appl Math 2018;80: 997-1002.
31. Ge SX, Jung D, Yao R. ShinyGO: a graphical gene-set enrichment tool for animals and plants. Bioinformatics 2020;36: 2628-29.
32. Olivier M, Goldgar DE, Sodha N, Ohgaki H, Kleihues P, Hainaut P, et al. Li-Fraumeni and related syndromes: correlation between tumor type, family structure, and TP53 genotype. Cancer Res 2003;63: 6643-50.
33. Bray F, Ferlay J, Soerjomataram I, Siegel RL, Torre LA, Jemal A. Global cancer statistics 2018: GLOBOCAN estimates of incidence and mortality worldwide for 36 cancers in 185 countries. CA Cancer J Clin 2018;68: 394-424.

34. Bouaoun L, Sonkin D, Ardin M, Hollstein M, Byrnes G, Zavadil J, et al. TP53 variations in human cancers: new lessons from the IARC TP53 database and genomics data. Hum Mutat 2016;37: 865-76.
35. Brennan CW, Verhaak RG, McKenna A, Campos B, Noushmehr H, Salama SR, et al. The somatic genomic landscape of glioblastoma. Cell 2013;155: 462-77.
36. Tate JG, Bamford S, Jubb HC, Sondka Z, Beare DM, Bindal N, et al. COSMIC: the catalogue of somatic mutations in cancer. Nucleic Acids Res 2019;47: D941-D47.
37. Baugh EH, Ke H, Levine AJ, Bonneau RA, Chan CS. Why are there hotspot mutations in the TP53 gene in human cancers? Cell Death Differ 2018;25: 154-60.
38. Alexandrova EM, Mirza SA, Xu S, Schulz-Heddergott R, Marchenko ND, Moll UM. p53 loss-of-heterozygosity is a necessary prerequisite for mutant p53 stabilization and gain-of-function in vivo. Cell Death Dis 2017;8: e2661.
39. Liu DP, Song H, Xu Y. A common gain of function of p53 cancer mutants in inducing genetic instability. Oncogene 2010;29: 949-56.
40. Wang X, Sun D, Tai J, Chen S, Yu M, Ren D, et al. TFAP2C promotes stemness and chemotherapeutic resistance in colorectal cancer via inactivating hippo signaling pathway. J Exp Clin Cancer Res 2018;37: 27.
41. Xu A, Yang H, Gao K, Zhan Z, Song Z, Huang T, et al. Expression profiles and prognostic significance of WNT family members in glioma via bioinformatic analysis. Biosci Rep 2020;40: BSR20194255.
42. Ostrom QT, Cioffi G, Gittleman H, Patil N, Waite K, Kruchko C, et al. CBTRUS statistical report: primary brain and other central nervous system tumors diagnosed in the United States in 2012-2016. Neuro Oncol 2019;21: v1-v100.
43. Lopes-Ramos CM, Chen CY, Kuijjer ML, Paulson JN, Sonawane AR, Fagny M, et al. Sex differences in gene expression and regulatory networks across 29 human tissues. Cell Rep 2020;31: 107795.
44. Kolat D, Kaluzinska Z, Bednarek AK, Pluciennik E. The biological characteristics of transcription factors AP-2alpha and AP-2gamma and their importance in various types of cancers. Biosci Rep 2019;39: BSR20181928.
45. Binda E, Visioli A, Giani F, Trivieri N, Palumbo O, Restelli S, et al. Wnt5a drives an invasive phenotype in human glioblastoma stem-like cells. Cancer Res 2017;77: 996-1007.
46. Rosini P, Bonaccorsi L, Baldi E, Chiasserini C, Forti G, De Chiara G, et al. Androgen receptor expression induces FGF2, FGF-binding protein production, and FGF2 release in prostate carcinoma cells: role of FGF2 in growth, survival, and androgen receptor down-modulation. Prostate 2002;53: 310-21.
47. Jimenez-Pascual A, Hale JS, Kordowski A, Pugh J, Silver DJ, Bayik D, et al. ADAMDEC1 maintains a growth factor signaling loop in cancer stem cells. Cancer Discov 2019;9: 1574-89.
48. Zhao N, Wang F, Ahmed S, Liu K, Zhang C, Cathcart SJ, et al. Androgen receptor, although not a specific marker for, is a novel target to suppress glioma stem cells as a therapeutic strategy for glioblastoma. Front Oncol 2021;11: 616625.